JOURNAL OF MATERIALS PROCESSING TECHNOLOGY 199 (2008) 214–220

journal homepage: www.elsevier.com/locate/jmatprotec

An upper-bound analysis of the tube extrusion process

R. Ebrahimi[a,*], M. Reihanian[b], M. Kanaani[a], M.M. Moshksar[a]

[a] Department of Materials Science and Engineering, School of Engineering, Shiraz University, Shiraz, Iran
[b] Department of Materials Science and Engineering, Faculty of Engineering, Shahid Chamran University, Ahwaz, Iran

ARTICLE INFO

Article history:
Received 5 July 2006
Received in revised form
17 July 2007
Accepted 30 July 2007

Keywords:
Upper-bound theory
Tube extrusion
Optimum die angle
Friction

ABSTRACT

In this paper a new upper-bound approach is used to analyze the tube extrusion process. A kinematically admissible velocity field is developed to evaluate the internal power and the power dissipated on frictional and velocity discontinuity surfaces. The total power is optimized with respect to the die angle. The optimum die angle and the critical die angle at which a dead zone is formed are determined. The effect of constant friction factor and reduction in area on the optimum die angle is predicted. In addition, the role of die angle on the relative extrusion pressure is investigated. Comparison of the experimental and theoretical load–displacement curves shows a good agreement.

1. Introduction

Extrusion is a bulk metal forming process in which the cross-sectional area of a billet is reduced and changed to a desired shape by forcing it through a die. One of the main applications of the extrusion process is the manufacturing of seamless tubes in a wide range of reductions and materials, known as tube extrusion. Tube extrusion is extensively used for producing hollow complex shaped products (Moshksar and Ebrahimi, 1998, 1999; Bae and Yang, 1993a,b). It is also suitable for manufacturing of composite tubes (Chitkara and Aleem, 2001a). Several attempts have been made to analyze the tube extrusion process, using finite elements method (FEM) (Reddy et al., 1996), slip line method (Chitkara and Butt, 1999), slab method (Chitkara and Aleem, 2001b) and upper-bound theory (Mehta et al., 1970; Chang and Choi, 1972; Hartley, 1973; Altan, 1994). The upper-bound theory is the most important analytical method that may be lead to individual equations in metal forming analysis. Mehta et al. (1970) obtained a velocity field for tube extrusion and compared it to the experimental velocity fields using the viso-plasticity method. Chang and Choi (1972) used the upper-bound solution for tube extrusion through curved dies and studied the effect of die geometry and friction. They also treated the tube extrusion process through conical dies of small angle as an illustration. Hartley (1973) proposed a kinematically admissible velocity field for tube extrusion which reduces to a kinematically admissible velocity field for solid rods extrusion in the limit as the mandrel diameter goes to zero. Altan (1994) assumed the straight flow lines and proposed a deformation model for tube extrusion through a flat die.

In this paper a new upper-bound analysis is used for tube extrusion process. A kinematically admissible velocity field is developed and the effect of process variables on the relative extrusion pressure is investigated. Based on this model, the equation for optimum die angle, dead zone cone angle and relative extrusion pressure are derived. For comparing the theoretical results to that of experimental results, a tube

* *Corresponding author.*
E-mail address: ebrahimy@shirazu.ac.ir (R. Ebrahimi).
0924-0136/$ – see front matter © 2007 Elsevier B.V. All rights reserved.
doi:10.1016/j.jmatprotec.2007.07.034

Nomenclature

k	shear yield stress of the material
L_f	contact length of die at exit channel
L_0	contact length of billet at entrance channel
m	constant friction factor
P_{ext}	extrusion pressure
r, θ, ϕ	spherical coordinates
r_f	spherical radius of exit velocity discontinuity surface
r_0	spherical radius of entrance velocity discontinuity surface
R_i	radius of mandrel (internal radius of tube)
R_f	radius of exit channel (external radius of tube)
R_0	radius of container
S	area of frictional or velocity discontinuity surface
Δv	amount of velocity discontinuity
V_f	exit velocity
V_0	entrance velocity
$\dot{U}_r, \dot{U}_\theta, \dot{U}_\phi$	velocity components in spherical coordinates
$\dot{w}_i$	power dissipated in the deformation zone
$\dot{w}_S$	power dissipated on the frictional or discontinuity surface

Greek symbols

α_{crt}	critical angle at which a dead metal zone is formed
α_{opt}	optimum die angle
α_1	optimum dead zone formation angle
$\dot{\varepsilon}_{ij}$	strain rate tensor
σ_0	mean flow stress of the material

extrusion die with an orthogonal semi-die angle and a mandrel connected to the ram is designed and used for the experimental works.

2. Analysis of deformation

Based on the upper-bound theory, for a rigid-plastic Von-Misses material and amongst all the kinematically admissible velocity fields, the actual one that minimizes the power required for material deformation is expressed as

$$J=2k\int_V\sqrt{\frac{1}{2}\dot{\varepsilon}_{ij}\dot{\varepsilon}_{ij}}\,dV+\int_{S_v}k\,\Delta v\,dS+\int_{S_f}mk\,\Delta v\,dS-\int_{S_t}T_i v_i\,dS \quad (1)$$

where k is the shear yield stress of the material, $\dot{\varepsilon}_{ij}$ the strain rate tensor, m the constant friction factor, V the volume of plastic deformation zone, S_v and S_f the area of velocity discontinuity and frictional surfaces respectively, S_t the area where the tractions may occur, Δv the amount of velocity discontinuity on the frictional and discontinuity surfaces and v_i and T_i are the velocity and tractions applied on S_t, respectively.

Fig. 1 shows the deformation model considered for this analysis. As shown, the volume considered for analysis is divided into four regions. In regions I and III the material moves rigidly with the velocity V_0 and V_f, respectively. Region II is the deformation zone in which the material undergoes plastic deformation and region IV is a dead metal zone. Regions I, II and III are separated by the velocity discontinuity surfaces S_1 and S_2. In addition to these surfaces, there are some frictional surfaces between mandrel surface, die walls and material (S_4–S_7).

Region IV appears as a dead metal zone, when the semi-cone angle, α, becomes larger than a critical value, α_{crt}. In this case surface S3 acts as a velocity discontinuity surface. For the semi-cone die angle smaller than a critical value, α_{crt}, surface, S_3, appears as a frictional die surface.

Using spherical coordinates (r, θ, ϕ), it is assumed that the material in the deformation zone only has a radial component of velocity field, $\dot{U}_r$, and the other two components of the velocity field are zero ($\dot{U}_\theta = \dot{U}_\phi = 0$).

In order to determine the radial component of velocity field, $\dot{U}_r$, a differential element moving in the radial direction is considered (Fig. 1). From volume constancy, the flow rate through a differential area at any arbitrary radius r from the center O must be equal to the flow rate through a differential area on the surface S_1. That is

$$2\pi(R_i + r\sin\theta)r\,d\theta(-\dot{U}_r) = 2\pi(R_i + r_f\sin\theta)r_f\,d\theta(V_f\cos\theta) \quad (2)$$

where r_f is spherical radius of exit velocity discontinuity surface. Then $\dot{U}_r$ can be obtained as

$$\dot{U}_r = -V_f\frac{r_f(R_i + r_f\sin\theta)}{r(R_i + r\sin\theta)}\cos\theta \quad (3)$$

For small diameter of the mandrel, Eq. (3) is simplified as

$$\dot{U}_r \cong -V_f\frac{r_f^2}{r^2}\cos\theta \quad (4)$$

Due to the assumed velocity field in the deformation zone, the strain rate tensor in the spherical coordinates is determined as

$$\dot{\varepsilon}_{rr} = \frac{\partial\dot{U}_r}{\partial r} \cong V_f\frac{2r_f^2}{r^3}\cos\theta \quad (5)$$

$$\dot{\varepsilon}_{\theta\theta} = \dot{\varepsilon}_{\phi\phi} = \frac{\dot{U}_r}{r} \cong -V_f\frac{r_f^2}{r^3}\cos\theta \quad (6)$$

$$\dot{\varepsilon}_{r\theta} = \frac{1}{2}\left(\frac{1}{r}\frac{\partial\dot{U}_r}{\partial\theta}\right) \cong \frac{V_f}{2}\frac{r_f^2}{r^3}\sin\theta \quad (7)$$

The internal power dissipated in the deformation zone is given by

$$\dot{w}_i = \frac{2}{\sqrt{3}}\sigma_0\int_V\sqrt{\frac{1}{2}\dot{\varepsilon}_{ij}\dot{\varepsilon}_{ij}}\,dV \quad (8)$$

where σ_0 is the mean flow stress of the material and dV is a differential volume in the deformation zone:

$$dV = 2\pi(R_i + r\sin\theta)r\,dr\,d\theta \quad (9)$$

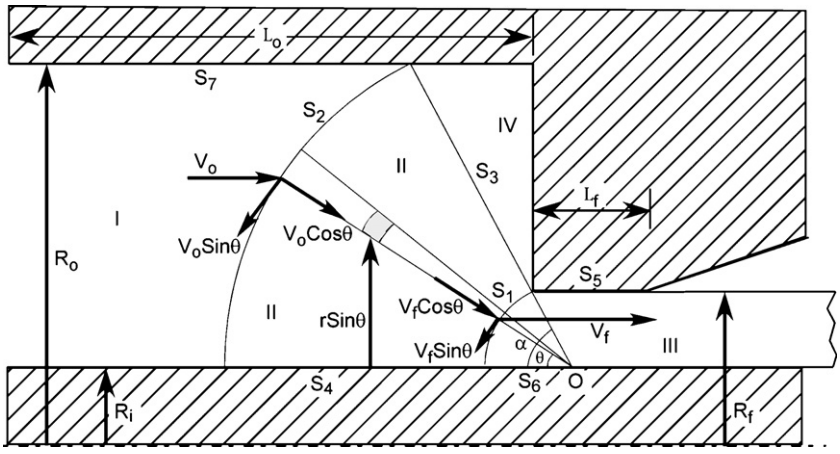

Fig. 1 – Deformation model considered for tube extrusion process.

Substituting the strain rate tensor, from Eqs. (5)–(7), and the differential volume, from Eq. (9), into Eq. (8), the internal power becomes

$$\dot{w}_i = \frac{4\pi}{\sqrt{3}}\sigma_0 \int_{r_f}^{r_0}\int_0^{\alpha} \sqrt{\left(3V_f^2\frac{r_f^4}{r^6}\cos^2\theta + \frac{V_f^2}{4}\frac{r_f^4}{r^6}\sin^2\theta\right)} (R_i + r\sin\theta) r\,dr\,d\theta \quad (10)$$

From the geometry of deformation we have

$$r_0 = \frac{R_0 - R_i}{\sin\alpha} \quad (11)$$

$$r_f = \frac{R_f - R_i}{\sin\alpha} \quad (12)$$

$$V_f = \frac{R_0^2 - R_i^2}{R_f^2 - R_i^2} V_0 \quad (13)$$

By integrating Eq. (10) and using Eqs. (11)–(13), the internal power in the deformation zone is determined as

$$\dot{w}_i = 4\pi\sigma_0 V_0 \frac{(R_0 - R_f)(R_0 + R_i)}{(R_f + R_i)} R_i + 2\pi\sigma_0 V_0 \frac{(R_0^2 - R_i^2)(R_f - R_i)}{(R_f + R_i)} \ln\left(\frac{R_0 - R_i}{R_f - R_i}\right) f(\alpha) \quad (14)$$

where

$$f(\alpha) = \frac{1}{\sin^2\alpha}\left(1 - \cos\alpha\sqrt{1 - \frac{11}{12}\sin^2\alpha} + \frac{1}{\sqrt{11\times 12}}\ln \times \left(\frac{1 + \sqrt{11/12}}{\sqrt{11/12}\cos\alpha + \sqrt{1 - (11/12)\sin^2\alpha}}\right)\right) \quad (15)$$

It should be noted that for integration of the first term of Eq. (10), the approximation of $11/12 \approx 1$ is assumed.

The power dissipated on the velocity discontinuity surfaces S_1 and S_2 is given by

$$\dot{w}_S = \int_S k\,\Delta v\,dS \quad (16)$$

where for velocity discontinuity surface S_1:

$$\Delta v_1 = V_f \sin\theta \quad (17)$$

$$dS_1 = 2\pi(R_i + r_f\sin\theta) r_f\,d\theta \quad (18)$$

For velocity discontinuity surface S_2:

$$\Delta v_2 = V_0 \sin\theta \quad (19)$$

$$dS_2 = 2\pi(R_i + r_0\sin\theta) r_0\,d\theta \quad (20)$$

By using Eqs. (11)–(13) and inserting (17)–(20) in Eq. (16), the power dissipated on the velocity discontinuity surfaces S_1 and S_2 are determined as

$$\dot{w}_{S_1} = 2\pi\frac{\sigma_0}{\sqrt{3}}\left(\frac{R_0^2 - R_i^2}{R_f + R_i}\right) V_0 \times \left(\frac{2\sin\alpha - \cos\alpha\sin\alpha - \alpha}{2\sin^2\alpha} R_i + \frac{\alpha - \cos\alpha\sin\alpha}{2\sin^2\alpha} R_f\right) \quad (21)$$

$$\dot{w}_{S_2} = 2\pi\frac{\sigma_0}{\sqrt{3}}(R_0 - R_i) V_0 \times \left(\frac{2\sin\alpha - \cos\alpha\sin\alpha - \alpha}{2\sin^2\alpha} R_i + \frac{\alpha - \cos\alpha\sin\alpha}{2\sin^2\alpha} R_0\right) \quad (22)$$

The power dissipated on the surface S_3 depends on whether the semi-cone angle, α, is larger or smaller than the critical semi-cone angle, α_{crt}. When α is smaller than α_{crt}, surface S_3 acts as a frictional surface and the power dissipated on it

becomes

$$\dot{w}_S = \int_S mk\,\Delta v\,dS \tag{23}$$

where m is the constant friction factor. For frictional surface S_3:

$$\Delta v_3 = |\dot{U}_r|_{\theta=\alpha} = V_f \frac{r_f(R_i + r_f \sin\alpha)}{r(R_i + r\sin\alpha)} \cos\alpha \tag{24}$$

$$dS_3 = 2\pi(R_i + r\sin\alpha)\,dr \tag{25}$$

Thus:

$$\dot{w}_{S_3} = 2\pi \frac{m\sigma_0}{\sqrt{3}} V_f \cos\alpha (R_i + r_f \sin\alpha) r_f \int_{r_f}^{r_0} \frac{dr}{r} \tag{26}$$

By integrating Eq. (26) and using Eqs. (11)–(13), the power dissipated on the frictional surface S_3 is obtained as

$$\dot{w}_{S_3} = 2\pi \frac{m\sigma_0}{\sqrt{3}} V_0 \frac{(R_0^2 - R_i^2)R_f}{(R_f + R_i)} (\cot\alpha) \ln\left(\frac{R_0 - R_i}{R_f - R_i}\right) \tag{27}$$

When α is larger than α_{crt}, a dead-zone forms and surface S_3 acts as a discontinuity surface and Eq. (27) is replaced by

$$\dot{w}_{S_3} = 2\pi \frac{\sigma_0}{\sqrt{3}} V_0 \frac{(R_0^2 - R_i^2)R_f}{(R_f + R_i)} (\cot\alpha) \ln\left(\frac{R_0 - R_i}{R_f - R_i}\right) \tag{28}$$

The power dissipated on the frictional surfaces S_4–S_7 is also obtained by Eq. (23). Because the mandrel moves with a velocity of V_0, the velocity discontinuity on surface S_4 and its area becomes

$$\Delta v_4 = |\dot{U}_r|_{\theta=0} - V_0 = \frac{r_f}{r} V_f - V_0 \tag{29}$$

$$dS_4 = 2\pi R_i\,dr \tag{30}$$

For frictional surface S_5:

$$\Delta v_5 = V_f \tag{31}$$

$$\Delta S_5 = 2\pi R_f L_f \tag{32}$$

For frictional surface S_6:

$$\Delta v_6 = V_f - V_0 \tag{33}$$

$$\Delta S_6 = 2\pi R_i r_f = 2\pi R_i \left(\frac{R_f - R_i}{\sin\alpha}\right) \tag{34}$$

Finally for frictional surface S_7:

$$\Delta v_7 = V_0 \tag{35}$$

$$\Delta S_7 = 2\pi \left(L_0 - \frac{R_0 - R_f}{\tan\alpha}\right) R_0 \tag{36}$$

Then by replacing Eqs. (29)–(36) into Eq. (23) and using Eqs. (11)–(13), the power dissipated on the frictional surfaces S_4–S_7 can be determined as

$$\dot{w}_{S_4} = 2\pi \frac{m\sigma_0}{\sqrt{3}} V_0 R_i \left(\frac{R_0^2 - R_i^2}{(R_f + R_i)\sin\alpha} \ln\left(\frac{R_0 - R_i}{R_f - R_i}\right) - \frac{R_0 - R_f}{\sin\alpha}\right) \tag{37}$$

$$\dot{w}_{S_5} = 2\pi \frac{m\sigma_0}{\sqrt{3}} V_0 \left(\frac{R_0^2 - R_i^2}{R_f^2 - R_i^2}\right) R_f L_f \tag{38}$$

$$\dot{w}_{S_6} = 2\pi \frac{m\sigma_0}{\sqrt{3}} V_0 \left(\frac{R_0^2 - R_f^2}{R_f + R_i} - 1\right) R_i \tag{39}$$

$$\dot{w}_{S_7} = 2\pi \frac{m\sigma_0}{\sqrt{3}} V_0 \left(L_0 - \frac{R_0 - R_f}{\tan\alpha}\right) R_0 \tag{40}$$

Based on the model, the total power needed for tube extrusion process can be obtained by summing the internal power and the power dissipated on all frictional and velocity discontinuity surfaces. Then

$$\dot{w}_{total} = \dot{w}_i + \dot{w}_{S_1} + \dot{w}_{S_2} + \dot{w}_{S_3} + \dot{w}_{S_4} + \dot{w}_{S_5} + \dot{w}_{S_6} + \dot{w}_{S_7} \tag{41}$$

The total power in equation above is a function of semi-cone angle α. The optimum semi-cone angle, α_{opt}, that minimizes the total power, can be determined by differentiating the total power with respect to α and set the derivative equal to zero:

$$\frac{\partial \dot{w}_{total}}{\partial \alpha} = 0 \tag{42}$$

which yields:

$$\alpha_{opt} = \sqrt{\frac{(mR_f + mR_i)((R_0^2 - R_i^2)/(R_f + R_i))\ln((R_0 - R_i)/(R_f - R_i)) - mR_i(R_0 - R_f)}{((R_0^2 - R_i^2)/(R_f + R_i))((R_i/6) + (R_f/3)) + (R_0 - R_i)((R_i/6) + (R_f/3)) + (m/2)R_i((R_0^2 - R_i^2)/(R_f + R_i))\ln((R_0 - R_i)/(R_f - R_i)) - (m/2)R_i(R_0 - R_f)}} \tag{43}$$

In the case that a dead zone is formed, the dead zone cone angle, α_1, is determined by

$$\alpha_1 = \sqrt{\frac{(R_f + mR_i)((R_0^2 - R_i^2)/(R_f + R_i))\ln((R_0 - R_i)/(R_f - R_i)) - mR_i(R_0 - R_f)}{((R_0^2 - R_i^2)/(R_f + R_i))((R_i/6) + (R_f/3)) + (R_0 - R_i)((R_i/6) + (R_f/3)) + (m/2)R_i((R_0^2 - R_i^2)/(R_f + R_i))\ln((R_0 - R_i)/(R_f - R_i)) - (m/2)R_i(R_0 - R_f)}} \tag{44}$$

where it is assumed that $\partial f(\alpha)/\partial\alpha \approx 0$ (Avitzur, 1968), $\cos\alpha \approx 1 - \alpha^2/2$ and $\alpha\cot\alpha \approx 1 - \alpha^2/3$.The external power

for deformation of the material in tube extrusion process is given by

$$J^* = \pi(R_0^2 - R_i^2)V_0 P_{ext} \tag{45}$$

where P_{ext} is the extrusion pressure. By equating this power to the total power derived in Eq. (41), the relative extrusion pressure is determined as

$$\begin{aligned}\frac{P_{ext}}{\sigma_0} = {} & \frac{4(R_0 - R_f)R_i}{(R_0 - R_i)(R_f + R_i)} + \frac{2(R_f - R_i)}{(R_f + R_i)} \ln\left(\frac{R_0 - R_i}{R_f - R_i}\right) f(\alpha) \\ & + \frac{2}{\sqrt{3}(R_f + R_i)}\left(\frac{2\sin\alpha - \cos\alpha\sin\alpha - \alpha}{2\sin^2\alpha}R_i\right. \\ & \left. + \frac{\alpha - \cos\alpha\sin\alpha}{2\sin^2\alpha}R_f\right) \\ & + \frac{2}{\sqrt{3}(R_0 + R_i)}\left(\frac{2\sin\alpha - \cos\alpha\sin\alpha - \alpha}{2\sin^2\alpha}R_i\right. \\ & \left. + \frac{\alpha - \cos\alpha\sin\alpha}{2\sin^2\alpha}R_0\right) + \frac{2mR_f}{\sqrt{3}(R_f - R_i)}(\cot\alpha)\ln\left(\frac{R_0 - R_i}{R_f - R_i}\right) \\ & + \frac{2m}{\sqrt{3}\sin\alpha}\left(\frac{R_i}{R_f + R_i}\ln\left(\frac{R_0 - R_i}{R_f - R_i}\right) - \frac{R_i(R_0 - R_f)}{R_0^2 - R_i^2}\right) \\ & + \frac{2mR_f}{\sqrt{3}(R_f^2 - R_i^2)}L_f + \frac{2mR_i\left(R_0^2 - R_f^2\right)}{\sqrt{3}(R_f^2 - R_i^2)(R_0^2 - R_i^2)}L_f \\ & + \frac{2m}{\sqrt{3}}\left(L_0 - \frac{R_0 - R_f}{\sin\alpha}\right)\frac{R_0}{R_0^2 - R_i^2}\end{aligned} \tag{46}$$

3. Experimental procedures

A load–displacement curve was obtained experimentally to evaluate the theoretical results. To obtain the experimental load–displacement curve, an extrusion die with a die angle of 90° and a mandrel connecting to the ram was designed. Sample material used in this work was commercially pure Al, with inside and outside diameter of 6 and 20 mm, respectively, and length of 40 mm. The samples were machined from a rod and annealed at 420 °C for 3 h. Shaving foam was used for lubrication. The constant friction factor, m, appropriate for forming process was estimated by the "Barrel Compression Test" (Ebrahimi and Najafizadeh, 2004). Tests were carried out at the same temperatures and using the same lubricants as for tube extrusion process. A constant friction factor of about 0.1 was estimated. To determine the mean flow stress, the compression tests incorporating the Cook and Larke technique were used and a work hardening equation of the form below was obtained:

$$\sigma\,(\text{MPa}) = 195\varepsilon^{0.316} \tag{47}$$

Based on Eq. (47) a mean flow stress of 175 MPa was estimated for the material used.

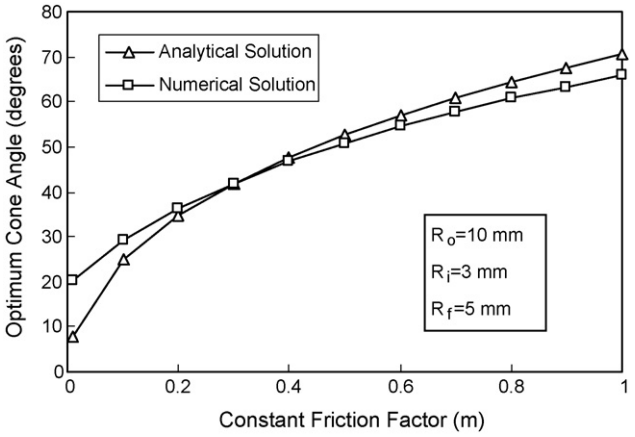

Fig. 2 – Effect of constant friction factor on the optimum semi-cone angle, α.

4. Results and discussion

In order to verify the validity of the approximations used in the analytical solutions, the problem was also solved numerically without any approximation by using the Simpson method.

The effect of constant friction factor, m, on the optimum semi-cone angle, α_{opt}, obtained from both analytical and numerical solutions is shown in Fig. 2. Good agreement is observed between the two solutions. The agreement between the numerical solution and the analytical solution indicates that the approximations used in the analytical method are quite reasonable. As shown in Fig. 2, with increasing the constant friction factor, m, the optimum die angle, α_{opt}, increases significantly. This arises from the fact that with increasing the constant friction factor, the area of some frictional surfaces decreases to minimize the power. This occurs by increasing the optimum semi-cone angle.

The effect of constant friction factor on the dead zone cone angle, α_1, obtained from analytical and numerical solutions, is shown in Fig. 3. Both solutions predict that the constant friction factor has no significant effect on the dead zone cone angle; so that with increasing the constant friction factor, dead zone cone angle increases only about 4%. It is a reasonable

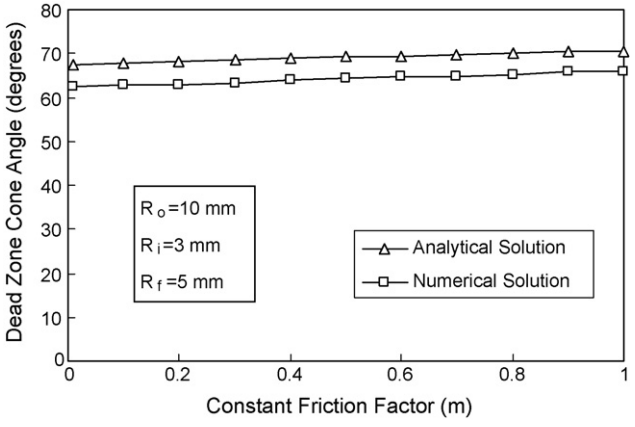

Fig. 3 – Effect of constant friction factor on the dead zone cone angle, α_1.

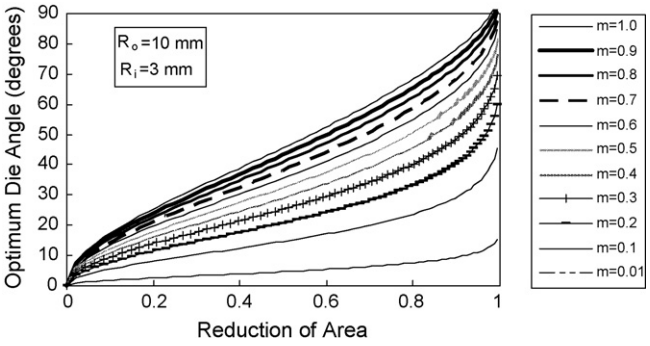

Fig. 4 – Effect of reduction in area on the optimum die angle, α_{opt}.

result, because in case of the dead zone formation, the area of frictional surfaces is decreased and the effect of constant friction factor is reduced.

Fig. 4 shows the effect of reduction in area on the optimum semi-cone angle for different values of m. With increasing the reduction in area, the optimum semi-cone angle increases. It should be noted that the effect of reduction in area is only significant at high values of m, because at low values of m, the area of frictional surfaces has no significant effect on the extrusion power.

The effect of die angle on the relative extrusion pressure is shown in Fig. 5 for different values of m. As it is expected, for a given value of m, there is an optimum die angle, at which the power is minimized. Also as discussed above, the optimum die angle increases with increasing the constant friction factor.

The critical die angle, α_{crt}, at which a dead metal zone is formed, can be easily determined by considering Fig. 6. This figure shows the effect of die angle on the relative extrusion pressure for the case of $m = 0.1$, $R_0 = 10$ mm, $R_i = 3$ mm and $R_f = 5$ mm. Based on Eq. (44), the dead zone cone angle, α_1, for this condition is 67.83°. If the total extrusion power is determined at this angle and superimposed on Fig. 6 (horizontal line), it will intersect with the curved line at an angle of 85.7°, which is the critical die angle for the dead zone formation.

In Fig. 7, the theoretical load–displacement curves obtained from the analytical and numerical solutions of the upper-bound approach are compared with the experimental results. The results show very good agreement between the theory and experiment. From these results, it can be concluded that the approximations used in the analytical solutions are construc-

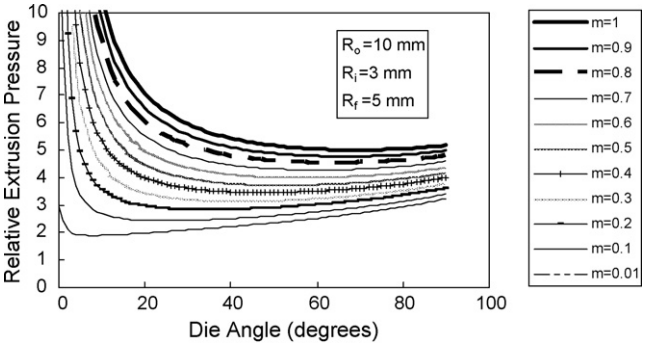

Fig. 5 – Effect of die angle on the relative extrusion pressure.

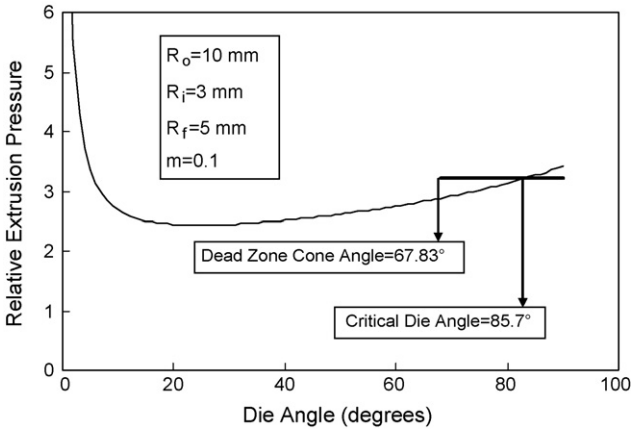

Fig. 6 – Determination of the critical die angle for dead zone formation.

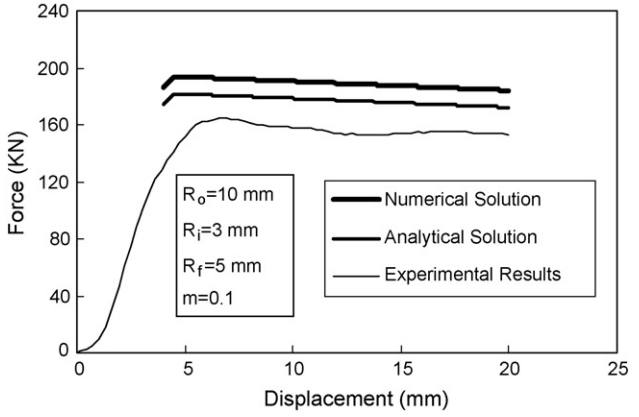

Fig. 7 – Comparison of the theoretical and experimental load–displacement curves.

tive. The gradual decrease in the load–displacement curves is because of decreasing the frictional surface area in the container as the punch is advanced. The theoretically predicted load is about 10% higher than the experimental results, which is due to the nature of the upper-bound theory.

5. Conclusions

A new upper-bound model is used to analysis the tube extrusion process and the following results are obtained:

(1) Comparison between the optimum semi-cone angle obtained by the numerical and analytical solutions confirms the validity of the analytical solutions. Also, the results of the theoretical and experimental load–displacement curves show very good agreement between the theory and experiment.
(2) For a given value of constant friction factor, there is an optimum die angle, α_{opt}, in which the power is minimized. The optimum die angle is derived as an individual equation.

(3) With increasing the constant friction factor, the optimum cone angle increases. However, the constant friction factor has no significant effect on the dead zone cone angle.
(4) With increasing the reduction in area, the optimum semi-cone angle increases. The effect of the reduction in area is much more significant at high values of constant friction factor.
(5) For die angles larger than a critical value, α_{crt}, a dead metal zone with a cone angle of α_1 is formed on the corner of the die.

Acknowledgment

Financial support by the office of Research Council of Shiraz University through grant number 84-EN-1768-C306 is appreciated.

REFERENCES

Altan, S.B., 1994. A deformation model for tube extrusion. J. Mater. Process. Technol. 40, 305–313.
Avitzur, B., 1968. Metal Forming: Processes and Analysis, first ed. McGraw-Hill, New York.
Bae, W.B., Yang, D.Y., 1993a. An upper-bound analysis of the backward extrusion of tubes of complicated internal shapes from round billets. J. Mater. Process. Technol. 36, 175–185.
Bae, W.B., Yang, D.Y., 1993b. An analysis of backward extrusion of internally circular-shaped tubes from arbitrarily shaped billets by the upper-bound method. J. Mater. Process. Technol. 36, 157–173.
Chang, K.T., Choi, J.C., 1972. Upper-bound solutions to tube extrusion problems through curved dies. ASME J. Eng. Ind. 94, 1108–1112.
Chitkara, N.R., Aleem, A., 2001a. Extrusion of axisymmetric bi-metallic tubes: some experiments using hollow billets and application of a generalized slab method of analysis. Int. J. Mech. Sci. 43, 2857–2882.
Chitkara, N.R., Aleem, A., 2001b. Extrusion of axisymmetric tubes from hollow solid circular billets: a generalized slab method of analysis and some experiments. Int. J. Mech. Sci. 43, 1661–1684.
Chitkara, N.R., Butt, M.A., 1999. Axisymmetric tube extrusion through a smooth conical or cosine die and over a conical or ogival mandrel: numerical construction of axisymmetric slip line fields and associated velocity fields. Int. J. Mech. Sci. 41, 1191–1215.
Ebrahimi, R., Najafizadeh, A., 2004. A new method for evaluation of friction in bulk metal forming. J. Mater. Process. Technol. 152, 136–143.
Hartley, C.S., 1973. Upper-bound analysis of extrusion of axisymmetric, piecewise, homogeneous tubes. Int. J. Mech. Sci. 15, 651–663.
Mehta, H.S., Shabaik, A.H., Kobayashi, S., 1970. Analysis of tube extrusion. ASME J. Eng. Ind. 92, 403–411.
Moshksar, M.M., Ebrahimi, R., 1998. An analytical approach for backward-extrusion forging of regular polygonal hollow components. Int. J. Mech. Sci. 40, 1247–1263.
Moshksar, M.M., Ebrahimi, R., 1999. A new upper bound analysis for prediction of load and flow pattern in backward extrusion forging. Iran. J. Sci. Technol. Trans. B 23, 251–266.
Reddy, N.K., Dixit, P.M., Lal, G.K., 1996. Analysis of axisymmetric tube extrusion. Int. J. Mach. Tool. Manuf. 36, 1253–1267.